Thermophysics and Aeromechanics, *2016*, *Vol. 23*, *No. 4*

DOI: 10.1134/S0869864316040016

Direct numerical simulation of the turbulent flows of power-law fluids in a circular pipe*

A.A. Gavrilov[1] and V.Ya. Rudyak[2]

[1]*Kutateladze Institute of Thermophysics SB RAS*, *Novosibirsk*, *Russia*

[2]*Novosibirsk State University of Architecture and Civil Engineering*, *Novosibirsk*, *Russia*

E-mail: valery.rudyak@mail.ru

(*Received August 6*, *2015*)

Fully developed turbulent pipe flows of power-law fluids are studied by means of direct numerical simulation. Two series of calculations at generalised Reynolds numbers of approximately 10000 and 20000 were carried out. Five different power law indexes n from 0.4 to 1 were considered. The distributions of components of Reynolds stress tensor, averaged viscosity, viscosity fluctuations, and measures of turbulent anisotropy are presented. The friction coefficient predicted by the simulations is in a good agreement with the correlation obtained from experiment. Flows of power-law fluids exhibit stronger anisotropy of the Reynolds stress tensor compared with the flow of Newtonian fluid. The turbulence anisotropy becomes more significant with the decreasing flow index n. An increase in apparent viscosity away from the wall leads to the damping of the wall-normal velocity pulsations. The suppression of the turbulent energy redistribution between the Reynolds stress tensor components observed in the simulations leads to a strong domination of the axial velocity pulsations. The damping of wall-normal velocity pulsations leads to a reduction of the fluctuating transport of momentum from the core toward the wall, which explains the effect of drag reduction.

Key words: non-Newtonian fluids, power-law fluids, turbulent flows, direct numerical simulation, flow in a circular pipe, turbulence anisotropy, viscosity pulsations.

Introduction

Turbulent flows of non-Newtonian viscoplastic and pseudo-plastic fluids in pipes and annular ducts are of significant practical importance because they are encountered in many industrial units (various heat exchangers, journal bearings, centrifuges, rock-drill mountings, rotational viscosimeters, etc.). The existing experimental data enable one to predict well the hydraulic drag coefficient in a pipe. To this end, one usually employs the experimental correlation [1]. However, this correlation is often not enough, especially at the description of complex flows. Despite the practical importance, the experimental data on such flows are very scarce. This is related, in particular, to the fact that most non-Newtonian fluids are optically not transparent, and one fails to use the laser Doppler anemometry for their investigation at the measurement of velocity fields. The availability of an extraordinarily complex and costly equipment is necessary for investigations with the aid of the nuclear magnetic resonance tomography, ultrasonic Doppler anemometry, etc., which in turn is also not universal.

* The work was partially supported by the Russian Science Foundation (Grant No. 14-19-00312).

The mathematical modeling is an alternative technique for obtaining the information about the flows under study (see, for example, [2–5] and the bibliography cited therein). So one succeeds in modeling of laminar flows. The turbulent flow regime is usually modeled on the basis of using the Reynolds-averaged equations of rheodynamics with the aid of the so-called RANS approach [6–10]. The fundamental difficulty arising here lies in the fact that the employed turbulence models cannot be verified directly on experimental data. Thus, the degree of the adequacy of obtained results remains unclear.

In the absence of systematic experimental data, the direct numerical simulation (DNS) is a tool, which gives the most complete and detailed pattern of turbulent flow. One needs, in particular, the statistical information about the structure of the flow of non-Newtonian fluids near the wall. Only three works are known until now, which are most interesting from the practical viewpoint and in which the flows of nonlinear viscoplastic fluids were investigated by the method of direct numerical simulation. In the first of them — the work [11] — the flow of a power-law fluid in a circular pipe was studied for several values of the fluid index and at the generalized Reynolds number of about 5500. The Herschel–Bulkley fluid flows were simulated later at the generalized Reynolds number equal to 7000 [12]. The influence of the fluid index on flow characteristics and the limit stress was investigated. The direct numerical simulation of the Herschel–Bulkley flow in an open channel was a continuation of these works [13]. The results of above computations were presented in the form of the mean velocity distributions, components of the tensor of Reynolds stresses, turbulence generation, fluctuations of the vorticity axial component, and the mean effective viscosity versus the distance from the wall. This is generally sufficient for the primary validation of RANS models of turbulence, which do not account for the correlation of viscosity fluctuations and shear rate. However, for constructing more complex and adequate models of turbulence, which account for viscosity fluctuations, one needs the information about the additional non-Newtonian stresses: the turbulence dissipation rate and the correlations of viscosity fluctuations with the velocity and the velocity gradient. The degree of turbulence anisotropy of the non-Newtonian fluid is generally higher than in the case of a Newtonian fluid. For this reason, the information about the balance of the components of the tensor of Reynolds stresses, which arise in the RANS models of turbulence of pseudo-plastic fluids, is also needed. And, finally, the advancement towards higher Reynolds numbers is necessary.

The purpose of the present work is the direct numerical simulation of the steady isothermal turbulent flows of power-law fluids with a given flow rate in a smooth pipe of circular cross section that is the fluids the stress tensor of which is determined by the relation $\boldsymbol{\tau} = \mu \mathbf{S}$, where $\mathbf{S} \equiv S_{ij} = (1/2)\left(\partial u_i / \partial x_j + \partial u_j / \partial x_i\right)$ is the tensor of strain rates, and the effective viscosity coefficient is determined by the relation

$$\mu = k_v \gamma^{n-1}, \tag{1}$$

here γ is the second invariant of the tensor of strain rates, $\gamma^2 = 2\mathbf{S} \cdot \mathbf{S} = 2S_{ij}^2$; k_v is the consistency factor, and n is the fluid index. The fluid indices were varied from 0.4 to 1. Two series of computations were executed: for Reynolds numbers Re = 10000 and 20000. The work presents the data on the distributions of the components of the tensor of turbulent stresses, viscosity fluctuations, turbulence anisotropy, and averaged viscosity.

1. Problem statement and numerical method

The isothermal flow of power-law fluids in a circular pipe is considered, which is governed by the following equations of rheodynamics:

$$\nabla \cdot \mathbf{u} = 0, \quad \rho(\partial \mathbf{u}/\partial t) + \rho \mathbf{u} \cdot \nabla \mathbf{u} = -\nabla p + \nabla \cdot (2\mu \mathbf{S}), \tag{2}$$

where $\mathbf{u}$ is the fluid velocity vector, ρ is the fluid density, p is the pressure. The viscosity coefficient entering here is determined by equation (1). The computational region is represented by a cylinder of a circular cross section with radius R = 1 m. Its base length amounts

to $L = 15R$, which is assumed sufficient for reproducing the turbulent statistics for Newtonian flows (see, for example, [14–16]).

A forced flow with a constant flow rate corresponding to the mean-mass velocity $U_m = 1$ m/s is specified in the duct. The periodic boundary conditions are posed at the inlet and outlet boundaries that is the velocity profile at the inlet boundary coincides at each moment of time with the velocity profile at the outlet boundary. The longitudinal pressure gradient is restored from the condition of ensuring a given flow rate.

The computational grid is multi-block and structured. For each series of computations with a given number $\mathrm{Re} = 2\rho R U_m / \mu_\mathrm{w}$, its own grid has been generated. Here μ_w is the mean viscosity coefficient on the wall, which is obtained in the process of computation by averaging the apparent viscosity field. The grid for a series of computations with the Reynolds number $\mathrm{Re} = 2\cdot10^4$ is generated from the grid for the series of computations with $\mathrm{Re} = 10^4$ by increasing the number of coordinate nodes by the factor of 1.8 in the radial and tangential directions and by the factor of 1.2 in the axial direction. The degree of grids refinement is presented in Table 1 in dimensionless units $\Delta x^+ = \Delta x / l_\tau$, where $l_\tau = \mu_\mathrm{w} / (\rho u_\tau)$ is the viscous length scale determined from the mean viscous friction on the wall τ_w, which is obtained from the equality $u_\tau = \sqrt{\tau_\mathrm{w} / \rho}$. The grid coordinate lines are clustered in the radial direction to the wall. Table 1 presents the grid step in the radial direction Δr^+ near the wall and at the duct center. The maximum grid step in the tangential direction $\Delta(r\theta)^+$ proves to be near the wall. All dimensionless lengths supplied with the superscript + have been normalized by l_τ here and in the following. The grid step Δz^+ is constant in the axial direction. The total number N of the cells of the employed grid is presented in the last column. The viscous Reynolds number $\mathrm{Re}_\tau = (\rho u_\tau R) / \mu_\mathrm{w}$, which has been determined in terms of viscous scales and the mean viscosity on the wall, is also used further at the representation of results.

At the initial moment of time, the random perturbations in the amount of several percents of the mean-mass velocity are imposed on the laminar Poiseuille profile. After the solution passage to the statistically steady regime, the integration of motion equations is carried out using the statistical information about the mean flow. The dimensionless time step equals $\Delta t^+ = \Delta t / t_\tau \sim 0.3$, which corresponds to the maximum Courant–Friedrichs–Lewy (CFL) number of less than 0.9. The time step is normalized by the time $t_\tau = \mu_\mathrm{w} / (\rho u_\tau^2) = \mu_\mathrm{w} / \tau_\mathrm{w}$. The statistics was gathered by averaging the temporal realizations and by averaging over the homogeneous spatial variables — along the axial z and azimuthal θ directions. As a result, the distributions along the radial direction r were formed. The minimum averaging time for all computations $T^+ = T / t_\tau \sim 4000$. The introduced averaging operation is denoted in the following by triangular parentheses ⟨⟩.

The consistency exponent was determined for each fluid characterized by index n preliminarily from the correlation for the drag coefficient [1] in such away that the given Re number is ensured. The drag coefficient (the friction on the wall) found as a result of computations differs from the correlation obtained in the work [1], and the computed value of the Re number also differs from the given value. Therefore, all computational results presented here are close in terms of the magnitude of the Re number, but may differ significantly in terms of the Re_τ value.

The numerical algorithm employed in the present work is based on the finite volume method for three-dimensional equations of fluid dynamics on the unstructured grid fitted to

Table 1

Finite-volume grid refinement

Re	Δr^+	$\Delta(r\theta)^+$ near the wall	Δz^+	N
10^4	from 0.5 to 5	8.7	10	$1.1\cdot10^7$
$2\cdot10^4$	from 0.5 to 5	8.7	15	$4.5\cdot10^7$

the computational region boundaries. The details of its implementation for simulating the lminar flows of the Newtonian, viscoplastic, and pseudo-plastic fluids have been described in detail in the works [5, 17–19]. The multi-block structured curvilinear grids are used for present computations. The convective terms of the momentum equation are approximated by a central high-order difference scheme [20]. The relation between the velocity and pressure fields, which ensures the satisfaction of the continuity equation, is realized with the aid of the SIMPLE-C procedure. The velocity and pressure values are determined at the centers of control volumes. To eliminate the pressure field oscillations the Rhie–Chow approach is used, which consists of a special interpolation of the velocity vector on the faces of control volumes. The unconditionally stable second-order Crank–Nicolson method is employed for the integration in time. Both the viscous and convective terms of the motion equation are approximated implicitly. To solve the difference equation for the pressure correction the method of conjugate residuals with preconditioning is used. A version of the incomplete LU factorization is employed as the preconditioner.

To speed up the computations the technology of parallel computations is applied, which is based on a decomposition of the computational region into several contacting subregions. The Message Passing Interface was employed as the communication library, which was realized in the library MPICH2. The computations were done on a cluster of six computers with quadrocore processors Intel Core I7 2600 and on the computer complex of the Information and Computer Center of the Novosibirsk State University with the use of 128 computer cores. The mean CPU time makes from several days to two weeks.

2. Validation and verification

One can find in the literature several works devoted to the direct numerical simulation of pipe flows [14–16, 21, 22]. In the present work, a direct numerical simulation of a turbulent flow of the Newtonian fluid in a pipe of circular cross section at the Reynolds number Re = = 5300 has been carried out for the computer code validation. The data of the direct numerical simulation [14, 22] were used as the benchmark data. The grid with $1.1 \cdot 10^7$ cells was used for the first computation. The size of cells in the radial direction was varied from 0.3 (in the l_τ units) near the wall to 2.5 at the duct center, and it was equal to 5 in the tangential direction near the wall, in the longitudinal direction (along the z coordinate) it was equal to 6.

The difference of the computed value of the drag coefficient from the values obtained in the works [14, 22] has proved less than 1 %. Figure 1 shows the distributions of the dimensionless velocity $U^+ = U_z / u_\tau$ and velocity fluctuations $u'^+ = u' / u_\tau$ versus the dimensionless distance from the duct wall along the radial direction $y^+ = (\rho y / \mu_w) u_\tau$ (y is the distance from the wall). The results are compared with the data of works [14, 22] and agree well with them.

At the DNS modeling of the channel flow, the question on the adequacy of the choice of the computational region length and the spatial fineness of the computational grid is of fundamental importance. One can respond to the question about the sufficiency of the channel length by analyzing the behavior of two-point correlations of the streamwise velocity along the axial direction. The distributions of two-point coefficients of the streamwise velocity correlations

$$R(u'_z u'_z)(z) = \frac{\langle u'_z(z_0) u'_z(z_0 + z) \rangle}{\sqrt{\langle u'^2_z(z_0) \rangle} \sqrt{\langle u'^2_z(z_0 + z) \rangle}},$$

where the averaging is made in time, are shown in Fig. 2. The data are presented for power-law fluids at n = 0.5, 0.6, 0.8 and Re = 10^4. The channel middle lies at z = 7.5R. The correlation was computed at the channel center at r = 0. An analysis of the behavior of the correlator data shows that at n = 0.6 and 0.8, the velocity correlations between the inlet cross section and

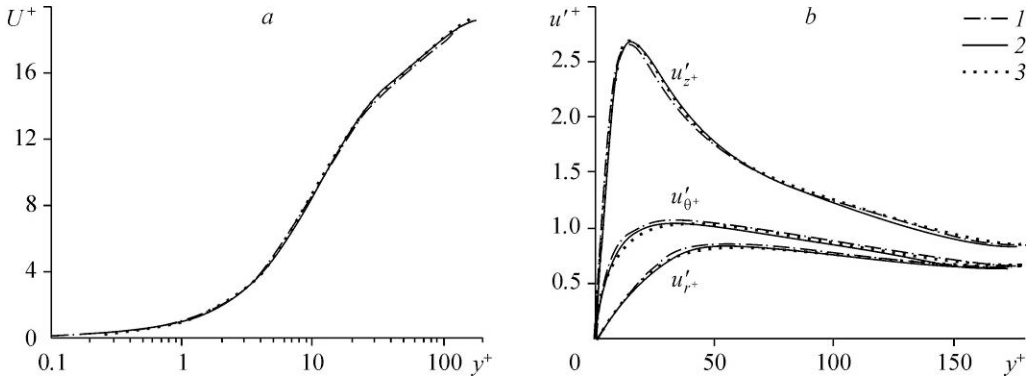

Fig. 1. Distributions of the mean velocity (*a*) and velocity fluctuations (root-mean-square deviations) (*b*).
Data of the works [14] (*1*), [22] (*2*) and the present work at $\mathrm{Re}_\tau = 180$ (*3*).

the cross section in the channel middle rapidly decay. Consequently, the channel length is in this case quite sufficient for modeling. On the other hand, at $n = 0.5$, the correlations do not decay, and in order to obtain the adequate result for this fluid, it is necessary to increase the computational region length.

The grid fineness and the time step size, which were chosen theoretically for computations (see the foregoing section) are sufficient for a DNS computation. However, the fluctuations of the viscosity coefficient take place in the power-law fluid (1) besides the usual fluctuations of hydrodynamic variables. It is, therefore, necessary to study the influence of these fluctuations on local resolution. To this end, the verification computations were done for a flow of the power-law fluid with $n = 0.6$ at the Reynolds number $\mathrm{Re} = 10^4$ on two grids. The first of them has been described in detail in section 1, we call it the base grid, and the second grid contained 45 million cells, and the time step was two times less than in the base grid case so that the maximum CFL number was below unity. The size of cells of this grid was varied in radial direction from 0.3 near the wall to 3 at the channel center; in the tangential direction near the wall, the cell size was equal to 5, and in the streamwise direction, it was equal to 8. It was found that at the use of a coarse grid, the integral drag coefficient has proved to be by 1.2 % lower than at the computation on a fine grid. The further data of these verification runs are shown in Fig. 3. The distributions of the velocity and velocity fluctuations (Figs. 3*a* and 3*b*) practically coincide, which was to be expected. Minor discrepancies are observed in the distributions of turbulent stresses (Fig. 3*c*) — there is only a small overestimation of the turbulent shear stress maximum (within 4 %). A similar behavior is observed also for the distribution of the dimensionless dissipation rate of the turbulent energy $\varepsilon^+ = \mu\varepsilon/(\rho u_\tau^4)$, where ε is the dissipation rate of the turbulent energy (see Fig. 3*d*). However, the differences prove to be here even less. Thus, the base grid refinement over the space is sufficient for

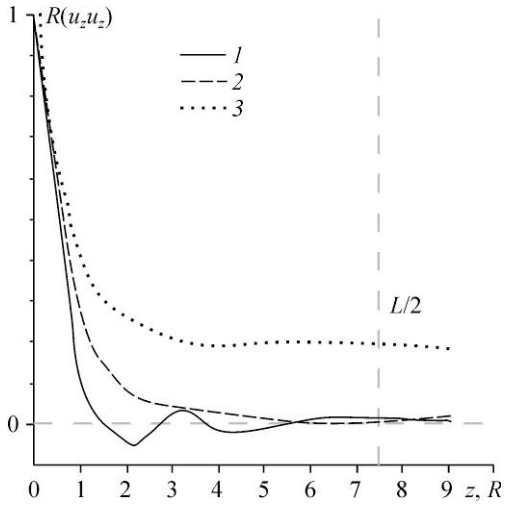

Fig. 2. Distributions of the coefficients of two-point correlations of the streamwise velocity, which are plotted along the channel axis.
$n = 0.8$ (*1*), 0.6 (*2*), 0.5 (*3*) at $\mathrm{Re}_\tau = 307$.

executing the direct numerical simulation of the turbulent flow of a non-Newtonian medium. A further reduction of the grid step will not lead to a significant alteration of results.

3. Results of the direct numerical simulation

The first series of runs was done for power-law fluids with indices n = 0.8, 0.7, 0.6, 0.5, and 0.4 at the Reynolds number near 10000 (see Table 2). This corresponded to the viscous Reynolds number $\mathrm{Re}_\tau \sim 310$. At the power exponent n = 0.4, the flow laminarization occurred, therefore, the results for n = 0.4 are not presented in the following.

Figure 4 shows the simulation results in the form of the distributions of various characteristics of the flows under consideration versus the dimensionless distance y^+ along the radial direction from the wall to the duct center. All presented data are normalized as before. The data for the turbulent flow of a Newtonian fluid for the same Reynolds number ($\mathrm{Re}_\tau = 310$) are also presented here.

In the mean velocity graphs (Fig. 4*a*), one can see well the viscous, puffer, and logarithmic layers. In the viscous sublayer region, the mean velocity profile remains linear and coincides for all studied fluids. The mean velocity profile of non-Newtonian fluids deviates from the Newtonian one starting from the coordinate value $y^+ > 10$. In the logarithmic layer, mean velocity values of non-Newtonian fluids lie above the corresponding values for the Newtonian fluid, and this difference enhances with decreasing index of the power-law fluid. The velocity inclination angle in the logarithmic sublayer differs more with decreasing fluid index from the value for the Newtonian fluid. This apparently points to the fact that for the non-Newtonian fluids, the turbulence is not fully developed, and a transitional flow regime is observed.

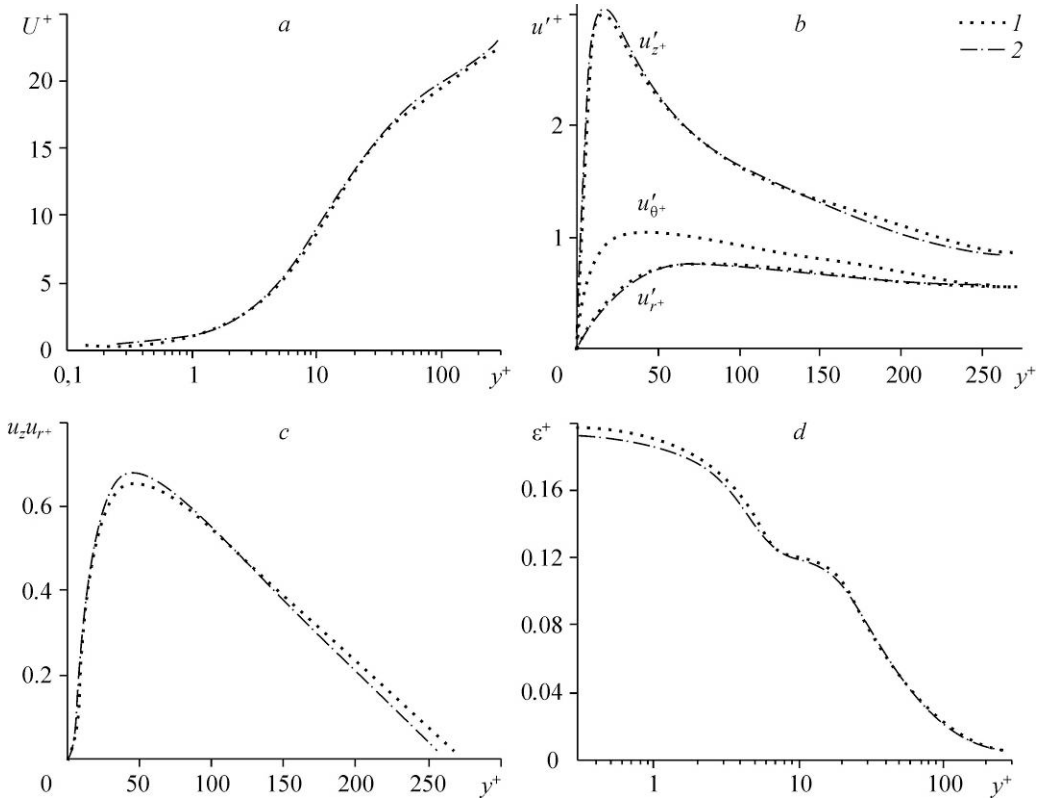

Fig. 3. Results of the verification run for $\mathrm{Re}_\tau \sim 270$ at n = 0.6 on the fine (*1*) and coarse (*2*) grids.

a — mean velocity, *b* — fluctuations of the velocity components,
c — turbulent shear stresses, *d* — dissipation rate of turbulent energy.

Table 2

Parameters of computations for Re = 10^4

n	Re	$\mathrm{Re}_{\mathrm{MR}}$	Re_τ	f_{DM}	f	Δf, %
1.0	10000	10000	307	$7.7\ 10^{-3}$	$7.55\ 10^{-3}$	2
0.8	9800	7010	292	$7.4\ 10^{-3}$	$7.09\ 10^{-3}$	4
0.7	9600	5900	280	$7.15\ 10^{-3}$	$6.8\ 10^{-3}$	5
0.6	9400	5100	267	$6.8\ 10^{-3}$	$6.42\ 10^{-3}$	6
0.5	9200	4500	251	$6.3\ 10^{-3}$	$6.0\ 10^{-3}$	5

With reducing fluid index n, the fluctuations of the radial and tangential velocity components decrease (Figs. 4*b* and 4*c*), and the maximum value of fluctuations drops by a factor of about two as compared with the corresponding value for a Newtonian fluid. On the contrary, the fluctuations of the streamwise velocity component increase (Fig. 4*d*), although the cross-correlations (turbulent shear stresses) decrease (Fig. 4*e*). An increase in the anisotropy of fluctuations is related to a reduction of the energy transfer from the axial fluctuations to the transverse ones. The fluctuations of the axial velocity component are generated in the near-wall flow, and then the turbulent energy of axial fluctuations is transferred with the aid of pressure fluctuations to two other components. In the case of a non-Newtonian fluid flow, this mechanism of energy transfer proves to be suppressed, which just leads to an increase of the level of axial fluctuations and a decrease of the radial and tangential fluctuations of the velocity. The growth of axial fluctuations leads to an increase in integral fluctuations, and, consequently, in the kinetic energy of turbulent fluctuations (see Fig. 4*f*, where $k^+ = k/u_\tau^2$ is the dimensionless mean kinetic energy of turbulent fluctuations (turbulent energy), and k is the dimensional one). An increase in the integral fluctuations is observed in the entire near-wall layer up to $y^+ \sim 100$, however, the kinetic energy of fluctuations drops in the flow core.

The reduction of turbulent shear stresses with reducing exponent of the fluid index occurs because of the drop of the intensity of fluctuations normal to the wall (radial fluctuations). The location of the maximum of stresses shifts from the wall to the flow region core (Fig. 4*e*), and the intensity of the mechanism of the momentum transfer from the flow core to the near-wall layer decreases.

Table 2 presents the integral parameters of conducted computations. For convenience, the third column of this table contains the generalized Reynolds numbers, which are generally employed for describing the flows of power-law fluids (Metzner–Reed, [23]):

$$\mathrm{Re}_{\mathrm{MR}} = \rho U_m^{2-n} D^n \Big/ \left(8^{n-1} k_\nu \left(\frac{3n+1}{4n} \right) \right),$$

where D is the pipe diameter. The fifth column contains the values of the drag coefficient $f_{\mathrm{DM}} = \tau_{\mathrm{w}} / (\rho U^2 / 2)$, which were obtained from the experimental correlation [1] (Dodge–Metzner), and the sixth column presents the values of f computed in the present work. Finally, the last column indicates the relative deviation of the computed value of the drag coefficient from the experimental correlation Δf. For all considered power-law fluids, the numerical drag coefficient is less than the corresponding value for the Newtonian fluid. This reduction is related to a reduction of the turbulent transfer of momentum and increases with decreasing fluid index. At n = 0.5, the differences exceed 20 %. Besides, the data of direct numerical simulation are systematically lower than the values obtained in the work [1], although these differences are below 6 %, which is within the accuracy of the correlation itself.

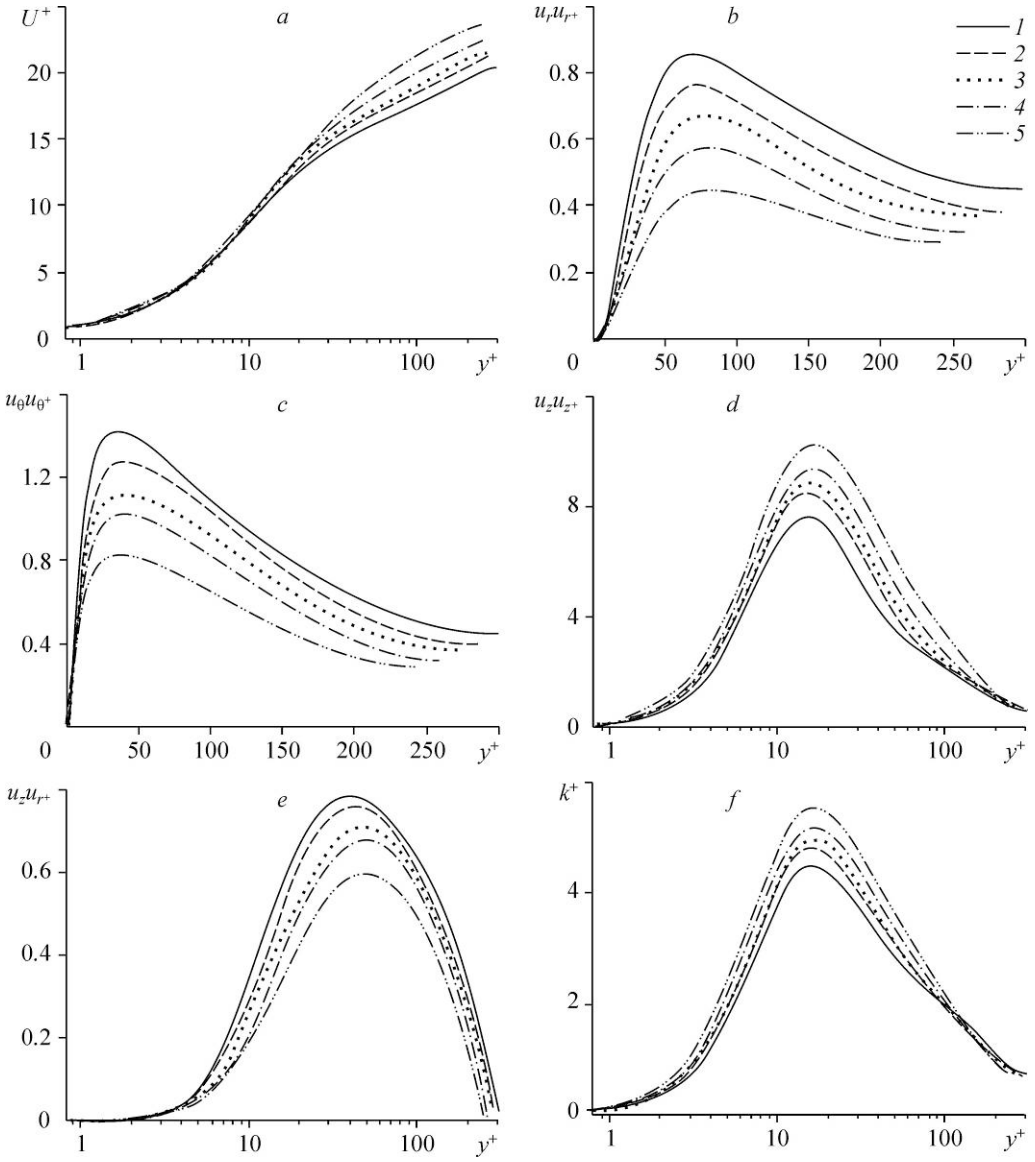

Fig. 4. Numerical results for Re_τ ~310.
a — mean axial velocity, *b*–*e* — the components of the tensor of turbulent stresses, *f* — the turbulence kinetic energy; *n* = 1 (*1*), 0.8 (*2*), 0.7 (*3*), 0.6 (*4*), 0.5 (*5*).

As was already noted, the second series of runs was done for the fluid indices n = 0.8, 0.6, and 0.4. For the Newtonian fluid, this corresponded to the Reynolds number Re = 20000 or the viscous Reynolds number Re_τ = 560. The corresponding Reynolds numbers for power-law fluids are given in Table 3. The integral results in the drag coefficient computation agree with the correlation of [1] practically with the same accuracy as for a lower Reynolds number (see Tables 2 and 3). The other modeling results are also qualitatively close.

Figure 5*a* shows the distributions of the mean axial velocity along the channel radius. The universal law of the wall $U^+ = 2.5\ln\left(y^+\right)+5.5$ has been also plotted here, which describes the mean velocity in a developed logarithmic layer for the flows with small Reynolds numbers. A comparison with the universal profile enables us to identify the subregions

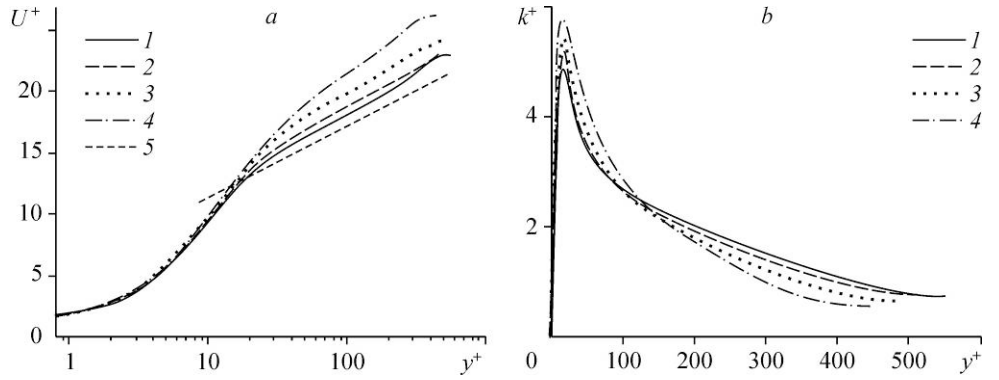

Fig. 5. Numerical results for a flow at Re = $2 \cdot 10^4$.

a — mean axial velocity, *b* — kinetic energy of turbulence;
n = 1 (*1*), 0.8 (*2*), 0.6 (*3*), 0.4 (*4*), the universal law of the wall (*5*); $\mathrm{Re}_\tau = 560$.

of a turbulent near-wall layer. The figure also shows well the viscous, puffer, and logarithmic layers. The qualitative behavior of presented distributions is seen to be practically the same as at Re = 10^4. For the media with *n* = 1.0, 0.8, and 0.6, the inclination angle in the logarithmic sublayer is the same. The velocity profiles for power-law fluids lie above the Newtonian profile. In the viscous sublayer region, the mean velocity profile remains linear for all fluids. As in the case of flows with Re = 10^4, the deviation of the inclination angle of the mean velocity profile is due to a substantial contribution of viscous stresses in the logarithmic sublayer. For a power-law fluid flow with *n* = 0.4, viscous stresses reach the values of 40–60 % of the turbulent stresses in the logarithmic sublayer. In this case, there is a non-developed turbulent flow.

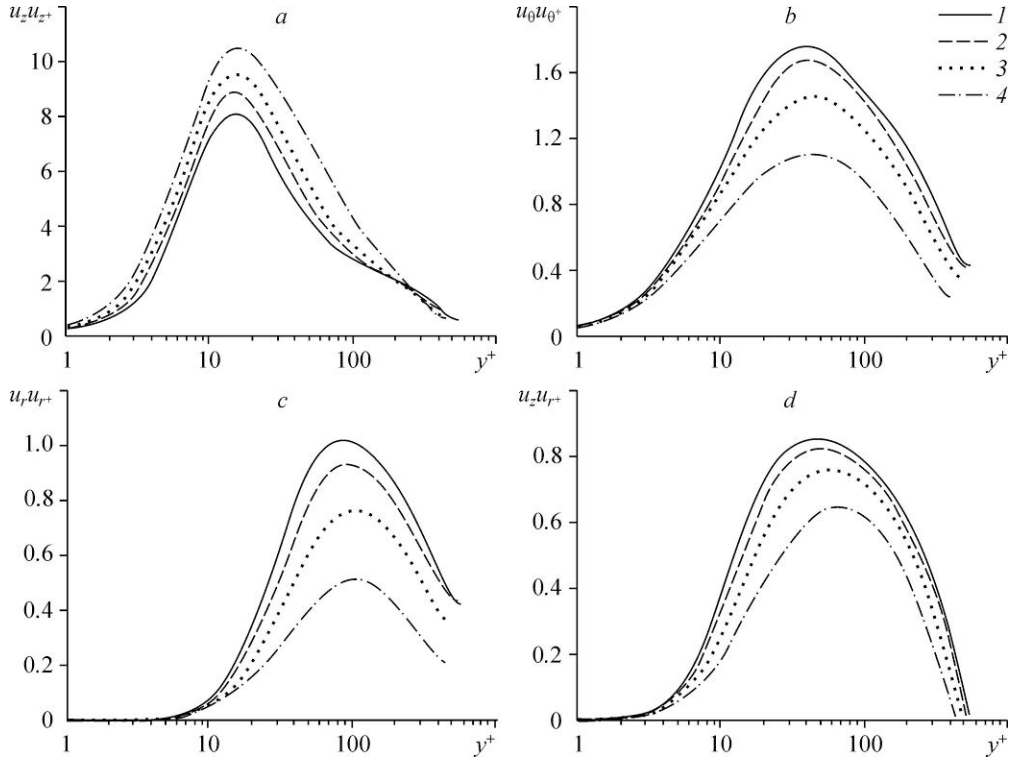

Fig. 6. Components of the tensor of turbulent stresses for the series Re = $2 \cdot 10^4$.

n = 1 (*1*), 0.8 (*2*), 0.6 (*3*), 0.4 (*4*).

Table 3

Parameters of computations for Re = $2 \cdot 10^4$

n	Re	Re_{MR}	Re_τ	f_{DM}	f	Δf, %
1.0	20000	20000	560	$6.48 \cdot 10^{-3}$	$6.27 \cdot 10^{-3}$	3
0.8	19460	12570	530	$6.28 \cdot 10^{-3}$	$5.96 \cdot 10^{-3}$	5
0.6	18760	8220	492	$5.86 \cdot 10^{-3}$	$5.5 \cdot 10^{-3}$	6
0.4	18150	5860	446	$5.0 \cdot 10^{-3}$	$4.84 \cdot 10^{-3}$	3.3

As in the first series of runs, one observes an increase in the kinetic energy of turbulent fluctuations (Fig. 5*b*). The character of the variations of the tensor of turbulent stresses at a power exponent reduction is quite analogous to a character observed in the foregoing series of runs with Re = 10^4. In the power-law fluids compared with the Newtonian fluid, the mechanism of the turbulent energy redistribution from the axial fluctuations to the transverse ones (radial and tangential) is suppressed. At a decrease of the power exponent n, the axial fluctuations in the puffer sublayer are increasing (Fig. 6*a*), and the velocity fluctuations in the radial and tangential directions decrease significantly in the entire flow region (Figs. 6*b* and 6*c*). As a result, the turbulent transfer of the momentum in the radial direction is suppressed in the power-law fluid, and the location of the maximum of shear stresses shifts from the wall to the flow core (Fig. 6*d*). The intensity of the total kinetic energy of turbulence in the near-wall region (in the puffer sublayer) increase, however, it is also suppressed far from the wall.

The above-listed peculiarities are typical not only of the non-developed turbulent flows of the power-law fluid, to which one can refer the fluid flow with n = 0.4, but also of the fully developed turbulent flows (for fluids with indices n = 0.8 and 0.6). The growth of the anisotropy of turbulent fluctuations (see the next section) proves to be related to the processes occurring in the viscous and puffer sublayers, where the viscous stresses and, respectively, the viscosity fluctuations are of big importance.

4. Turbulence anisotropy

The considered flows of power-law fluids possess a higher anisotropy degree than the Newtonian fluid flows. A detailed analysis of the anisotropy degree of the turbulence of non-Newtonian fluid flows based on experimental data has been presented in the work [24]. It was shown experimentally that for polymer solutions reducing the drag, the turbulence anisotropy is very close to the axisymmetric turbulence.

One can estimate quantitatively the turbulence anisotropy degree with the aid of the second invariant $A_2 = a_{ij} a_{ij}$ and third invariant $A_3 = a_{ij} a_{jk} a_{ki}$ of the turbulence anisotropy tensor

$$a_{ij} = \frac{\left\langle u_i' u_j' \right\rangle}{k} - \frac{2}{3} \delta_{ij}.$$

The second invariant gives a direct estimate of anisotropy: the higher this parameter the more the anisotropy of fluctuations.

The locations of flows on the map of invariants $A_2 - A_3$ [25] for the case of Re ~ 10^4 are shown in Fig. 7. All computed lines lie in the feasibility region bounded by the lines of two-component turbulence (2-C) and axisymmetric turbulence (AT). The maximum of anisotropy parameters lies at $y^+ \sim 8$. For all near-wall flows in viscous sublayer, the turbulence anisotropy corresponds to the two-component limit, which is explained by the suppression of fluctuations in the direction to the wall (radial fluctuations).

With increasing degree of the non-Newtonian character of the fluid that is with decreasing index n, one observes two explicit alterations of the map of invariants. Firstly, the maximum

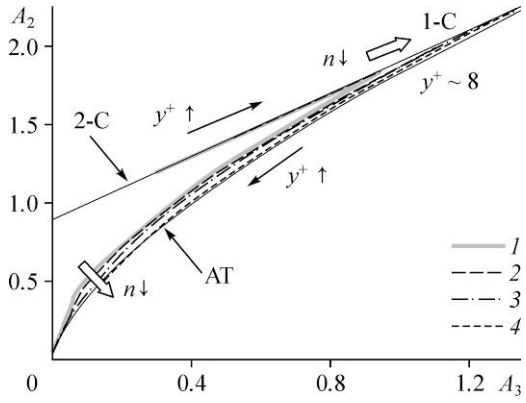

Fig. 7. Map of the invariants of the anisotropy tensor for flows with Re = 10^4. n = 1 (*1*), 0.8 (*2*), 0.6 (*3*), 0.4 (*4*).

values of the invariants A_2 and A_3 are increasing. The turbulence anisotropy tends to the one-component limit (1-C), which is due to the suppression of fluctuations in the azimuthal direction and the enhancement of fluctuations in axial direction in the puffer sublayer. Secondly, with decreasing index n, the dependence $A_2 - A_3$ tends to the line of axisymmetric turbulence (AT), at which the level of the fluctuations of the axial velocity component differs significantly (exceeds in our case) from the fluctuations of other components. Such a behavior agrees well with experimental data and is the key peculiarity of the flows of non-Newtonian fluids decreasing the drag [25].

The combination of the second and third invariants $A = 1 - 9(A_2 - A_3)/8$, which is known as the Lumley's flatness parameter [26], is convenient by that in the case of the isotropic three-dimensional turbulence, it is equal to unity, and in the case of the two-component turbulence that is when one of the normal components of the fluctuation tensor is equal to zero, equals zero. The distributions of this parameter versus the distance from the wall y^+ are shown in Fig. 8. The two-component turbulence with A = 0 forms in a direct proximity of the wall at $y^+ < 10$. The maximum of the parameter A_2 is observed at $y^+ \sim 8$. This maximum grows with decreasing index n. Note that the limiting value of the parameter A_2 corresponding to the one-component turbulence is equal to 8/3. An increase in the anisotropy degree with decreasing n is observed not only in the puffer sublayer but also in the logarithmic layer. Closer to the flow core, the values of A_2 for power-law fluids tend to the corresponding values for the Newtonian fluid. An isotropic turbulence with parameter A ~ 1 is typical of the flow core region.

With increasing Reynolds number the turbulence anisotropy degree A_2 of non-Newtonian fluids decreases in the near-wall layer (see Figs. 8*a* and 8*b*). For a non-Newtonian fluid, it proves nevertheless much higher than for the Newtonian fluid. The elevated degree of turbulence anisotropy of power-law fluids is a key peculiarity of their near-wall flows.

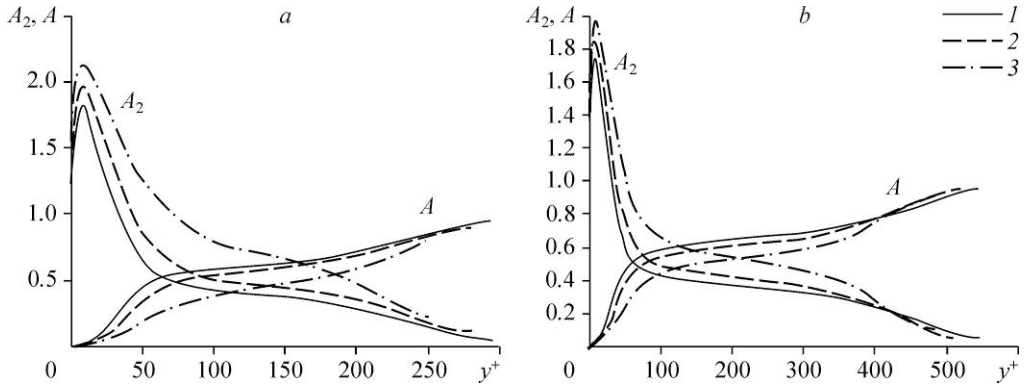

Fig. 8. Distribution of the invariants of the anisotropy tensor for Re = 10^4 (*a*) and $2 \cdot 10^4$ (*b*). n = 1 (*1*), 0.8 (*2*), 0.6 (*3*).

5. Averaged viscosity

In the works [11, 12], the mechanism of the suppression of the fluctuations normal to the wall is associated with an increase in the effective viscosity with increasing distance from the wall. One of the hypotheses explaining the suppression of turbulent exchange between the near-wall layer and the flow core in the flows of viscoelastic fluids is based on the elongation viscosity growth in the puffer layer (the so-called Metzner–Lumley mechanism [26, 27]). From this viewpoint, it is important to study the behavior of the effective viscosity coefficient and viscosity fluctuations depending on the distance from the wall.

The behavior of normalized values of the mean viscosity coefficient $\mu^+ = \langle\mu\rangle/\mu_w$ and the viscosity fluctuations $\tilde{\mu} = \mu'/[(1-n)\mu]$ depending on the distance from the wall is shown in Fig. 9. As was to be expected, for the power-law fluids, the normalized coefficient of the mean viscosity monotonously increases with increasing distance from the wall (Figs. 9*a* and 9*c*). In the region between the wall and $y^+ \geq 10$, the mean viscosity is nearly constant (Fig. 9*c*). Then (in region $y^+ \geq 10$) one observes a rapid growth of the mean viscosity coefficient. The ratio of the maximum (at the duct center) and minimum (on the wall) values of the viscosity coefficient increases with decreasing fluid index. At Re = $2\cdot10^4$, this ratio reaches the value of 14 for a medium with $n = 0.4$, and for a medium with $n = 0.6$, it is equal to about 4.

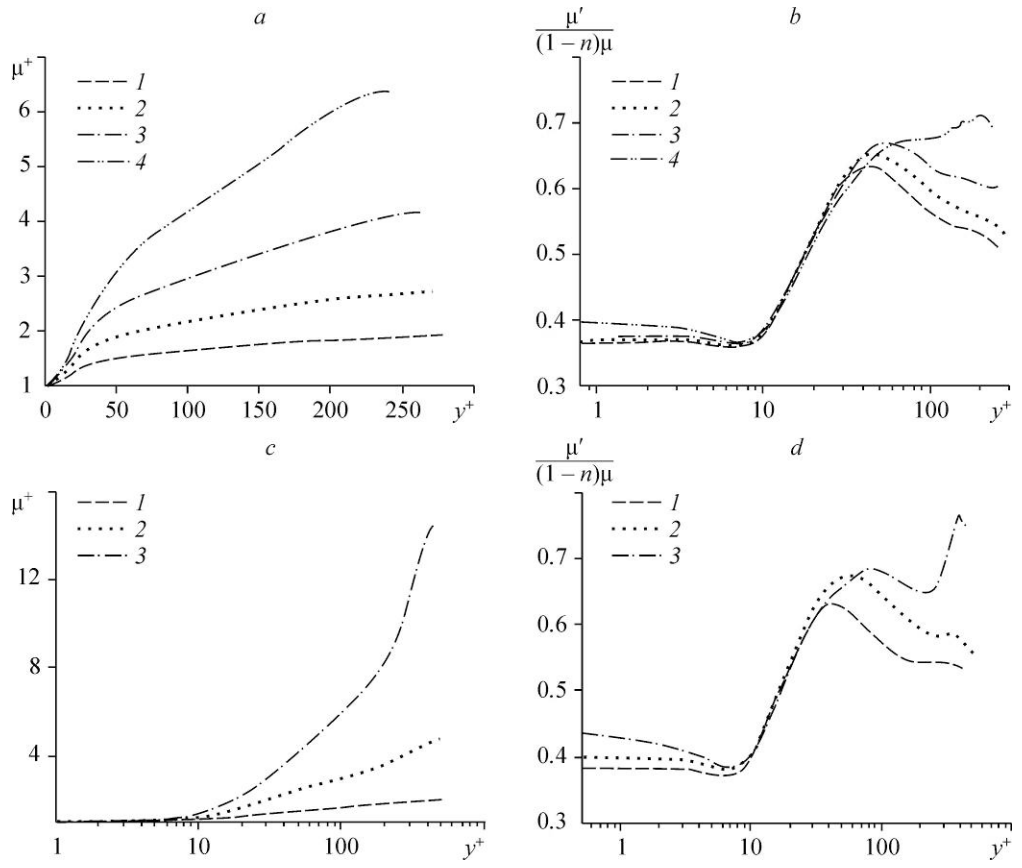

Fig. 9. Averaged viscosity and its fluctuation for Re = 10^4 (*a*, *b*), $2\cdot10^4$ (*c*, *d*).
a, *b* — n = 0.8 (*1*), 0.7 (*2*), 0.6 (*3*), 0.5 (*4*); *c*, *d* — n = 0.8 (*1*), 0.6 (*2*), 0.4 (*3*).

The distributions of relative fluctuations divided by the coefficient (1– n) are shown in Figs. 9*b* and 9*d*. The distribution of the fluctuations of the viscosity coefficient is non-monotonous. The viscosity fluctuations are significant not only in the flow core but also near the wall in the viscous sublayer region. For a power-law fluid in the regions of the viscous and puffer sublayers ($y^+ < 10$), the viscosity fluctuations are nearly constant and amount to about 10–20 % of the viscosity value on the wall. At $y^+ \sim 10$ (the region of a maximum generation of turbulence), a rapid growth of the averaged viscosity and viscosity fluctuations is observed. The maximum of fluctuations lies in the region $y^+ \sim 30 - 50$, at a further increase in the distance from the wall, the intensity of fluctuations is determined by the fluid index. It drops at $n \geq 0.6$, but at $n = 0.5$, it continues growing (Fig. 9*b*); for a flow with the Reynolds number $\mathrm{Re} = 2 \cdot 10^4$, the growth is observed at $n = 0.4$ (Fig. 9*d*). Thus, the magnitude of the viscosity fluctuations depends substantially on the fluid index, and it is higher for lower n. On the other hand, in the region of the viscous and puffer sublayer ($y^+ < 30$), the relative fluctuations of the viscosity are practically independent of the rheology.

Conclusion

The turbulent flow of non-Newtonian power-law fluids is characterized by a substantial diminution of the fluctuations normal to the wall, which leads to a reduction of the turbulent mechanism of the momentum transfer and fluctuations between the near-wall layer and the flow core. The viscosity increasing from the wall to the flow center leads to a damping of the fluctuations propagation from the region of their generation inside the flow. Turbulence is localized in the near-wall region.

One observes in the power-law fluid flows in channels the suppression of the mechanism of energy transfer from axial fluctuations to the transverse ones, which leads to the dominance of fluctuations in flow direction. The near-wall turbulence anisotropy is typical also of the developed turbulent flows of power-law fluids and is not related with a non-developed character of the logarithmic sublayer. The turbulence anisotropy of power-law fluid flows is much higher than in the case of conventional Newtonian fluids. Tending to the one-component limit near the wall (up to $y^+ \sim 10$) and to the limit of axisymmetric turbulence in the logarithmic sublayer is typical of it.

It is important to stress that the noted features of turbulent flows of power-law fluids are observed in the entire studied range of Reynolds numbers. It is clear from physical considerations that they will be observed also in the region of higher Reynolds numbers.

Note some differences from the results presented in [11, 12]. Unlike the work [11], in which large inexplicable differences (10–15 %) from experimental data for the drag coefficient have been obtained, the values obtained in the present work agree well with the experimental correlation, including the second series of runs at $\mathrm{Re} \sim 2 \cdot 10^4$. Unlike the works [11, 12], the results of the present work demonstrate for all considered Reynolds numbers an increase in axial fluctuations with increasing degree of the non-Newtonian character of the medium that is with decreasing fluid index. From the viewpoint of the turbulence anisotropy of the near-wall flow, the obtained data are close to the flows of viscoelastic media, in which a reduction of the turbulent flow drag is also observed. An increase in the turbulence anisotropy near the wall is explained by the suppression of the mechanism of redistributing the fluctuation energy between individual components of the Reynolds stress tensor.

References

1. **D.W. Dodge and A.B. Metzner,** Turbulent flow of non-Newtonian system, AIChE J., 1959, Vol. 5, No. 2, P. 189–204.
2. **M.P. Escudier, I.W. Gouldson, and D.M. Jones,** Flow of shear-thinning fluids in a concentric annulus, Experiments in Fluids, 1995, Vol. 18, P. 225–238.
3. **M.P. Escudier, P.J. Oliveira, and F.T. Pinho,** Fully developed laminar flow of purely viscous non-Newtonian liquids through annuli, including the effects of eccentricity and inner-cylinder rotation, Int. J. Heat and Fluid Flow, 2002, Vol. 23, P. 52–73.
4. **E.V. Podryabinkin and V.Ya. Rudyak,** Moment and forces exerted on the inner cylinder in eccentric annual flow, J. Engng Thermophys., 2011, Vol. 20, No. 3, P. 320–328.
5. **A.A. Gavrilov, A.V. Minakov, A.A. Dekterev, and V.Ya. Rudyak,** Numerical algorithm for fully developed laminar flow of non-Newtonian fluid through an eccentric annulus, Vychislitel'nye tekhnologii, 2012, Vol. 17, No. 1, P. 44–56.
6. **M.R. Malin,** Turbulent pipe flow of power-law fluids, Int. Communs. Heat Mass Transfer, 1997, Vol. 24, No. 7, P. 977–988.
7. **F.T. Pinho,** A GNF framework for turbulent flow models of drag reducing fluids and proposal for a k–ε type closure, J. Non-Newtonian Fluid Mech., 2003, Vol. 114, P. 149–184.
8. **D.O.A. Cruz and F.T. Pinho,** Turbulent pipe flow predictions with a low Reynolds number k–ε model for drag reducing fluids, J. Non-Newtonian Fluid Mech., 2003, Vol. 114, P. 109–148.
9. **A.A. Gavrilov and V.Ya. Rudyak,** Modeling the coefficient of molecular viscosity of viscoplastic fluids in turbulent regime, Doklady Academii Nauk Vysshei Shkoly of Russian Federation, 2013, No. 2, P. 69–80.
10. **A.A. Gavrilov and V.Ya. Rudyak,** A model of averaged molecular viscosity for turbulent flow of non-Newtonian fluids, J. Siberian Federal University. Mathematics and Physics, 2014, Vol. 7, No. 1, P. 46–57.
11. **M. Rudman, H.M. Blackburn, L.J.W. Graham, and L. Pullum,** Turbulent pipe flow of shear-thinning fluids, J. Non-Newtonian Fluid Mech., 2004, Vol. 118, P. 33–48.
12. **M. Rudman and H.M. Blackburn,** Direct numerical simulation of turbulent non-Newtonian flow using a spectral element method, Appl. Math. Modelling, 2006, Vol. 30, P. 1229–1248.
13. **R. Guang, M. Rudman, A. Chryss, P. Slatter, and S. Bhattacharya,** A DNS investigation of the effect of yield stress for turbulent non-Newtonian suspension flow in open channels, Particulate Sci. and Technology: An Int. J., 2011, Vol. 29, No. 3, P. 209–228.
14. **X. Wu and P. Moin,** A direct numerical simulation study on the mean velocity characteristics in turbulent pipe flow, J. Fluid Mech., 2008, Vol. 608, P. 81–112.
15. **N.V. Nikitin,** Direct numerical modeling of three-dimensional turbulent flows in pipes of circular cross section, Fluid Dyn., 1994, Vol. 29, No. 6, P. 749–758.
16. **N.V. Nikitin,** Statistical characteristics of wall turbulence, Fluid Dyn., 1996, Vol. 31, No. 3, P. 361–370.
17. **V.Ya. Rudyak, A.V. Minakov, A.A. Gavrilov, and A.A. Dekterev,** Application of new numerical algorithm for solving the Navier–Stokes equations for modelling the work of a viscometer of the physical pendulum type, Thermophysics and Aeromechanics, 2008, Vol. 15, No. 2, P. 333–345.
18. **A.A. Gavrilov, A.V. Minakov, A.A. Dekterev, and V.Ya. Rudyak,** Numerical algorithm for modeling laminar flows in an annular channel with eccentricity, J. Applied and Industr. Math., 2011, Vol. 5, No. 4, P. 559–568.
19. **V.Ya. Rudyak, A.V. Minakov, A.A. Gavrilov, and A.A. Dekterev,** Modelling of flows in micromixers, Thermophysics and Aeromechanics, 2010, Vol. 17, No. 4, P. 565–576.
20. **R. Rossi,** Direct numerical simulation of scalar transport using unstructured finite-volume schemes, J. Comput. Phys., 2009, Vol. 228, No. 5, P. 1639−1657.
21. **J.G.M. Eggels, F. Unger, M.H. Weiss, J. Westerweel, R.J. Adrian, R. Friedrich, and F.T.M. Nieuwstadt,** Fully developed turbulent pipe flow: a comparison between direct numerical simulation and experiment, J. Fluid Mech., 1994, Vol. 268, P. 175–181.
22. **K. Fukagata and N. Kasagi,** Highly energy-conservative finite difference method for the cylindrical coordinate system, J. Comput. Phys., 2002, Vol. 181, P. 478–498.
23. **A.B. Metzner and J.C. Reed,** Flow of non-Newtonian fluids – correlation of the laminar, transition and turbulent-flow regions, AIChE J., 1955, Vol. 1, No. 4, P. 434–440.
24. **M.P. Escudier, A.K. Nickson, and R.J. Poole,** Turbulent flow of viscoelastic shear-thinning liquids through a rectangular duct: Quantification of turbulence anisotropy, J. Non-Newtonian Fluid Mech., 2009, Vol. 160, P. 2–10.
25. **J.L. Lumley,** Computational modeling of turbulent flows, Adv. Appl. Mech., 1978, Vol. 18, P. 123–176.
26. **J.L. Lumley,** Drag reduction in two phase and polymer flows, Phys. Fluids, 1977, Vol. 20, P. S64–S65.
27. **A.B. Metzner,** Polymer solution and fiber suspension rheology and their relationship to turbulent drag reduction, Phys. Fluids, 1977, Vol. 20, P. S145–S146.